Astron. Astrophys. 351, 1075–1086 (1999)

ASTRONOMY AND ASTROPHYSICS

The abundances of O, S, Cl, N, Ar, He and C in seven Galactic H II regions⋆

M. Rodríguez

Instituto de Astrofísica de Canarias, 38200 La Laguna, Tenerife, Canarias, Spain (mrodri@ll.iac.es)

Received 12 July 1999 / Accepted 27 September 1999

Abstract. An analysis of CCD spectra in the range $\lambda\lambda 4200$–8775, obtained at several positions of seven bright Galactic H II regions, with galactocentric distances in the range 6–10 kpc, is presented. Temperatures, densities and ionic abundances are calculated for all the positions, and the relative trends followed by these parameters are established. It is shown that all these H II regions share the same abundances of O, S, Cl, N, Ar and He, within their expected uncertainties, a result which is consistent with a flat or small abundance gradient in the Galactic disc within ± 2 kpc from the Sun, as suggested by some studies of the abundances in H II regions and B-type stars. The same set of homogeneously derived ionic abundances is also used to test the accuracy of the fractional ionization predicted by available grids of models for photoionized nebulae.

Key words: ISM: H II regions – ISM: abundances – Galaxy: abundances

1. Introduction

One of the main sources of uncertainty in the determination of chemical abundances in H II regions is the correction for unseen ionization states. Two ionization correction schemes are usually used, the first one relies on empirically deduced formulae based on the similarity of ionization potentials for two distinct ions, whereas the second approach relies on the predictions of single ionization models that are assumed to reproduce the main characteristics of the observed object. The accuracy attained by these two approaches to derive total abundances varies from element to element and is difficult to estimate, thereby hampering a meaningful comparison of the chemical abundances determined for different objects, and consequently preventing an assessment of the accuracy of the derived Galactic abundance gradients.

The analysis presented here is based on CCD spectra obtained for seven of the brightest Galactic H II regions: M42, M43, M8, M16, M17, M20 and NGC 7635. This analysis centres on the emission lines not belonging to the Fe ions; the results related to the [Fe II] and [Fe III] lines and the Fe abundance are presented elsewhere (Rodríguez 1996, 1999, and a further paper currently in preparation). The spectra cover a relatively large wavelength range ($\lambda\lambda 4200$–8775) and allow the calculation of a homogeneous set of physical conditions and ionic abundances for several positions in H II regions with fairly different characteristics. This set of data is shown to imply that the seven H II regions share similar abundances within the expected errors. This result is inferred from the relative trends followed by the ionic abundances in all the positions; therefore it does not depend on any assumption for the contribution of the unobserved ions. Since the deduced common values for the chemical abundances in all the objects imply that the ionic abundances measured in each object are proportional to the ionization fraction of the corresponding ion, the observational results are compared to the predictions of grids of ionization models to assess their reliability.

2. Observations

Long-slit spectra covering the range $\lambda\lambda 4200$–8775 were obtained at the 2.5 m Isaac Newton Telescope on La Palma (Observatorio del Roque de los Muchachos, Canary Islands, Spain), equipped with the IDS spectrograph and a CCD detector. The full spectral range was covered with a spectral resolution of 4 Å using a grating of 632 lines mm^{-1} at three angles, and slit widths of $1\farcs4$ (1993 December) and $1\farcs5$ (1994 July). The observed objects, the positions and orientations (PA) of the slit, and the exposure times corresponding to the observed spectral ranges are listed in Table 1.

Bias frames, twilight and tungsten flat-field exposures, wavelength calibrations and exposures of standard stars (from the IRAF compilation) were taken each night. Sky spectra were obtained near each object after or before each set of nebular exposures.

3. Data reduction

The spectra were reduced to absolute intensity units using the IRAF reduction package, following standard procedures for the long-slit case. The overscan region in each frame and the bias

⋆ Based on observations made with the Isaac Newton Telescope, operated on the island of La Palma by the Isaac Newton Group in the Spanish Observatorio del Roque de los Muchachos of the Instituto de Astrofísica de Canarias.

Table 1. Journal of observations

Object	α (2000)	δ (2000)	PA	Date	Exposure times (s)		
	(hh mm ss)	(° ′ ″)	(°)		$\lambda\lambda$3985–5825	$\lambda\lambda$5180–7020	$\lambda\lambda$6970–8810
M42 A	05 35 15.9	−05 23 50	90	1993 Dec 12	3×1200, 300, 1	10, 120	2×1200, 300
M42 B	05 35 21.1	−05 24 38	59	1993 Dec 12,13	3×1200, 3, 1	20, 60	2×1200, 300
M43	05 35 28.8	−05 16 19	90	1993 Dec 13	3×1200	300	3×1800
					$\lambda\lambda$4200–5820	$\lambda\lambda$5615–7245	$\lambda\lambda$7140–8775
M8	18 03 41.5	−24 22 40	0	1994 Jul 8,9	2×1200, 300	300, 100, 10	3×1200
M16	18 18 50.0	−13 48 53	23	1994 Jul 10	4×1200	2×400, 200	4×1200
M17	18 20 42.0	−16 09 51	120	1994 Jul 9	3×1200, 300	500, 300, 200	3×1200
M20	18 02 28.2	−23 03 44	35	1994 Jul 11	3×1200	2×600	2×1200
NGC 7635	23 20 42.3	+61 11 27	118	1994 Jul 10,11	3×1200	600, 300, 180	3×1200

frames were used to remove the electronic pedestal level, its variations from frame to frame and the residual structure in the bias level.

The pixel-to-pixel gain variations were removed by using the tungsten flat-fields taken each night for each grating position; the twilight exposures were used to correct for the deviations of these lamp flat-fields from the slit illumination function.

The wavelength calibration was performed at different positions along the spatial axis, thus correcting for the optical distortions noticeable in the curvature of the slit image. The flux calibration was performed separately for each exposure, using the standard stars fluxes and the mean extinction curve for La Palma.

The sky emission lines were removed by subtracting the sky spectra after scaling them by factors of 0.5–1.5 to obtain the best cancellation. The equivalent nebular spectra were then combined to remove cosmic rays and to improve the signal-to-noise ratio. Some of the shortest nebular exposures were also retained, since some lines saturate in the longest exposures.

Sky subtraction is a critical step for most of the near-infrared lines. In general, all lines with $\lambda > 7200$ Å are affected because of the uncertainty contributed by sky emission to the continuum around the lines, but the biggest problems can arise for lines whose wavelengths are close to sky-emission lines: [O I] λ6300, [Ni III] λ7890, [Ar III] λ7751. Even relatively strong lines, like [O II] $\lambda 7320+30$, are affected by sky emission in some objects, like M16 and M20.

The stars appearing in most of the slit positions were used to estimate the possible spatial shifts of the slit image from one spectral range to another and across the same range: in all cases the misalignments remained to within one pixel. These stars were also used as references for extracting the spectra in several regions for each object, especially when the sum was performed over just a few pixels. Table 2 gives the positions and sizes of the selected regions, the nebular areas covered are indicated in Figs. 1 and 2 on reproductions of the seven H II regions.

Line intensities were measured by integrating between two given limits above a continuum fitted around each line. Blended lines, especially [Cl II] λ8579 and He I λ8583, were measured by fitting two Gaussian profiles of equal width, using the wavelength differences of the two components to constrain the fit. All these measurements were made using the *fitlines* routine implemented in IRAF by J. Acosta.

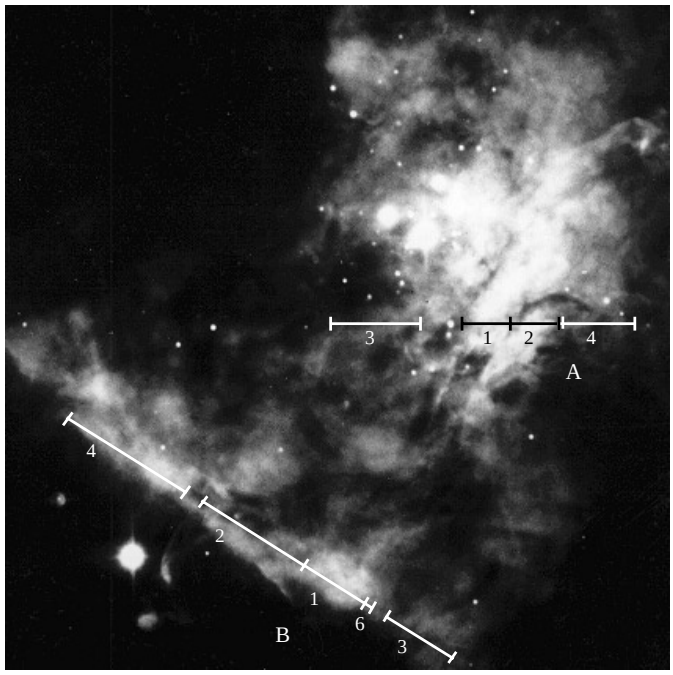

Fig. 1. Broad band Hα + [N II] image of the core of M42 (from Münch & Wilson 1962). The image size is about $3\farcm5 \times 3\farcm5$; north is at the top, west to the right. The Trapezium cluster – and θ^1 Ori C, the main ionizing star of the nebula – can be seen north of slit position A. The bright star south of the bar (slit position B) is θ^2 Ori A. The regions A–5 and A–6 are consecutive, cover 33″ each and are located west of the region A–4, with A–5 starting 7″ west of A–4. The region B–5 covers 24.″3 and starts 26″ from the end of B–4

The line intensities have been normalized to the brightest H I line appearing in the same spectral range: Hβ for the blue range, Hα for the red range and Pa12 or Pa13 for the near-infrared range. These line ratios, corrected for reddening (see Sect. 4 below), are used to determine the ionic abundances presented here. The tables listing the observed and reddening-corrected relative intensities for all lines of interest and each region considered are available on request to the author.

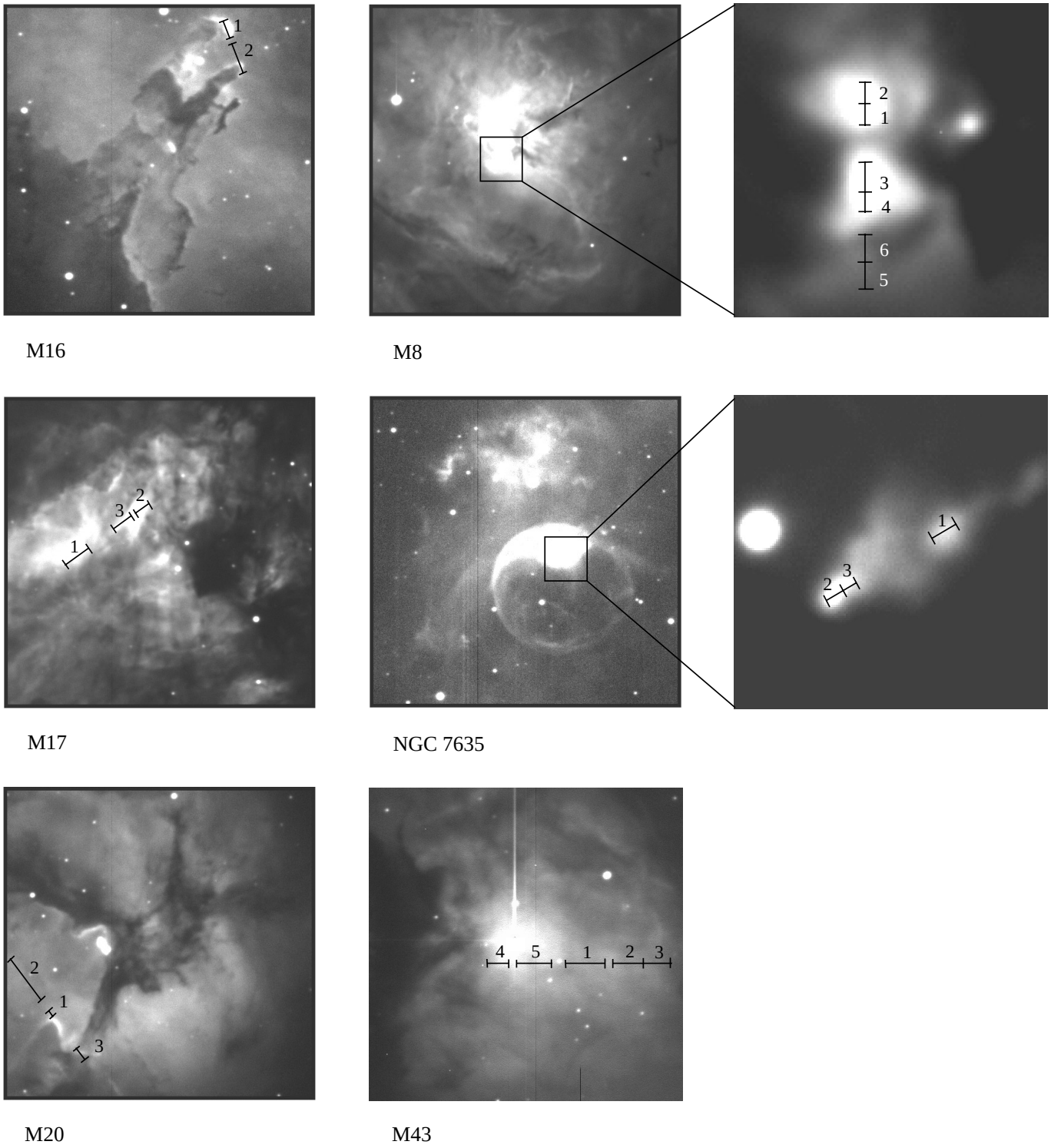

Fig. 2. $\mathrm{H}\alpha + [\mathrm{N\,II}]$ images of M16, M8, M17, NGC 7635, M20 and M43, along with the slit positions selected for each object. The size of the original images is $7' \times 7'$; north is at the top, west to the right. The images were obtained at the IAC80 telescope (Observatorio del Teide, Canary Islands, Spain). The image size for M43 is about $4' \times 4'$; this image was kindly obtained by M. Manteiga

4. Extinction correction

The extinction correction has been performed by interpolating Cardelli et al.'s (1989) R_V-dependent extinction law, with $R_V = A_V/E_{B-V}$, the ratio of visual extinction to colour-excess. The intensities measured for [N II] λ5754 in the blue and red spectral ranges have been used to bring the $\mathrm{H}\alpha$ and $\mathrm{H}\beta$ lines to the same scale. [The same correction factor has been applied to all the regions along each slit position, the maximum value

Table 2. Positions, sizes and extinction corrections

Object	Position[a] (″)	Size (″)	$I(\mathrm{H}\beta)$[b] $\times 10^{12}$	τ_β	R_V
M42 A–1	+14	13.4	19.4	1.40	5.5
M42 A–2	+27	13.4	20.1	1.40	5.5
M42 A–3	−25	26.2	23.9	2.10	5.5
M42 A–4	+42	16.6	16.0	1.20	5.5
M42 A–5	+74	32.6	19.4	1.20	5.5
M42 A–6	+107	32.6	8.84	1.10	5.5
M42 B–1	+30	24.3	29.3	1.90	7.0
M42 B–2	+0	34.6	31.4	1.80	7.0
M42 B–3	+64	25.0	18.5	1.50	5.5
M42 B–4	−44	46.7	47.0	1.90	7.0
M42 B–5	−105	24.3	8.31	1.50	4.5
M42 B–6	+43	3.2	2.95	1.80	5.5
M43–1	+21	28.8	2.03	1.55	5.5
M43–2	+63	26.2	1.42	1.45	5.5
M43–3	+89	25.6	0.59	1.54	5.5
M43–4	−54	17.9	2.01	1.60	6.0
M43–5	−16	23.0	1.97	1.63	6.0
M8–1	+0	4.8	1.81	3.10	7.0
M8–2	+5	4.2	2.04	2.90	7.0
M8–3	−10	4.8	1.90	2.50	7.0
M8–4	−14	3.6	1.04	2.30	5.5
M8–5	−28	6.0	0.54	2.20	5.0
M8–6	−22	6.0	0.70	2.70	7.0
M16–1	+7	15.0[c]	0.35	3.40	5.0
M16–2	+38	36.6	0.31	3.30	5.5
M17–1	−89	36.6	1.57	5.00	5.5
M17–2	+50	24.6	0.85	6.00	5.5
M17–3	+18	30.6	0.74	6.30	5.5
M20–1	−16	3.0	0.06	1.10	4.0
M20–2	−66	39.6	0.71	1.30	4.0
M20–3	+46	6.0	0.09	1.90	4.0
NGC 7635–1	+24	6.6	0.28	3.20	4.0
NGC 7635–2	+0	4.2	0.32	3.40	4.0
NGC 7635–3	+4	3.6	0.17	3.40	5.0

[a] Distance from the centre of each area to the slit positions listed in Table 1. Positive numbers indicate shifts to the west (to the north for M8)

[b] In erg cm^{-2} s^{-1}

[c] The selected region is 19.″2 wide, but the central 4.″2, containing a stellar spectrum, have been excluded

being of 10%.] The parameters R_V and τ_β (the effective optical depth for extinction at Hβ) have been fixed separately for each area by fitting the ratios $I(\mathrm{H}\gamma)/I(\mathrm{H}\beta)$ and $I(\mathrm{H}\alpha)/I(\mathrm{H}\beta)$ to their recombination values (Hummer & Storey 1987) for suitable physical conditions. The values of τ_β and R_V (listed in Table 2) are quite sensitive to calibration errors, and values as high as $R_V = 7$ are used for several positions, whereas Cardelli et al. (1989) derived their extinction law just for $2.5 < R_V < 6$. However, the values of the extinction parameters have no critical effect on the final results. We can obtain a highly conservative upper limit to the errors introduced by the extinction correction by considering the area most affected by extinction, M17–3, where $\tau_\beta = 6.3$ and $R_V = 5.5$ have been used. If $R_V = 7$ had been used instead – with $I(\mathrm{H}\gamma)/I(\mathrm{H}\beta)$ implying $\tau_\beta = 8.1$ – a drastic change to $R_V = 3.1$ (the mean value for the diffuse interstellar medium) and $\tau_\beta = 3.7$ would lead to a change of less than 50% (0.15 dex) in the ionic abundances derived here.

5. Physical conditions

Temperatures and densities were calculated with the *nebular* package implemented in IRAF, with the atomic parameters referenced therein (updated May 1997). The physical conditions were determined from intensity ratios that could be measured with precision, i.e. by comparing relatively bright lines that appear in the same wavelength range.

Electron densities have been obtained from the intensity ratios of the [S II] and [Cl III] lines $I(\lambda6716)/I(\lambda6731)$ and $I(\lambda5518)/I(\lambda5538)$; the derived values are listed in Table 3. Because of the weakness of the [Cl III] lines, the values of N_e[S II] are considered more reliable and are used hereafter to determine abundances.

The values of the temperatures T_e[O III] and T_e[N II] have been calculated from the intensity ratios $I(\lambda4959 + \lambda5007)/I(\lambda4363)$ and $I(\lambda6548 + \lambda6583)/I(\lambda5754)$, respectively, and are listed in Table 3.

Some of the abundance ratios derived here are very sensitive to temperature; hence, the accuracy of the values of T_e[O III] and T_e[N II] must be taken into account. The electron temperatures are affected by uncertainties of the atomic data (especially the collision strengths) and by observational errors. The uncertainty affecting existing atomic data cannot be estimated precisely, but the comparison of a given T_e[O III] and T_e[N II] with other values derived by different methods and numerical schemes, may provide an idea of the overall reliability of those values. In this paper the collision strengths of Lennon & Burke (1994) have been used to derive both temperatures. For comparison, the collision strengths of Baluja et al. (1980, 1981) for O^{++}, and those of Seaton (1975) and Stafford et al. (1994) for N^{+}, will be considered. All these calculations are based on the close-coupling approximation and on the configuration interaction method, but differ in the assumed ionic structure (the number of terms or states) and in the numerical procedures followed. The two sets of data for O^{++}, calculated for the same 12 ionic states, lead to essentially identical results for T_e[O III]. However, the calculations available for N^{+} are based on varied ionic representations: three terms (Seaton 1975), 12 terms (Lennon & Burke 1994) or 13 terms (Stafford et al. 1994). The results of Seaton (1975) are thought to be accurate within 10% (Mendoza 1983; Pradhan & Gallagher 1992), but the three sets of N^{+} collision strengths differ from each other up to $\sim$ 20% for some transitions and lead to differing T_e[N II]: the results of Lennon & Burke (1994) imply temperatures $\sim$ 200 K higher than those from Stafford et al. (1994) and $\sim$ 400 K higher than those of Seaton (1975). Referring to abundances, it should be borne in mind that a 6% uncertainty in both T_e[N II] and T_e[O III] (implied by 10% uncertainty in the collision strengths) translates into uncertainties

Table 3. Physical conditions

Object	N_e[S II] (cm^{-3})	N_e[Cl III] (cm^{-3})	T_e[N II] (K)	T_e[O III] (K)
M42 A–1	14600	10000	9700	8700
M42 A–2	12300	11900	10800	8800
M42 A–3	3500	6500	10000	8400
M42 A–4	5500	6800	10300	8600
M42 A–5	2500	2800	9400	8200
M42 A–6	1600	1700	10500	8400
M42 B–1	5000	5000	9400	8500
M42 B–2	3800	4600	9300	8500
M42 B–3	3100	3600	9300	8400
M42 B–4	3800	4100	9400	8600
M42 B–5	1500	1900	9100	8500
M42 B–6	5200	4600	9100	8200
M43–1	570	390	7900	...
M43–2	560	250	8000	...
M43–3	580	...	8000	...
M43–4	570	...	7800	...
M43–5	640	420	7800	...
M8–1	3200	5200	9300	8400
M8–2	1800	3100	8900	8000
M8–3	2000	3700	9000	8200
M8–4	1900	2400	8800	8200
M8–5	850	640	8500	8200
M8–6	1100	1200	9200	7900
M16–1	1400	1300	8500	...
M16–2	130	...	8800	...
M17–1	650	40	9100	8300
M17–2	740	330	9500	8100
M17–3	670	870	9200	8100
M20–1	360	280	8500	...
M20–2	120	...	8300	...
M20–3	340	1600	8600	...
NGC 7635–1	2800	3000	8600	...
NGC 7635–2	6200	4600	8900	...
NGC 7635–3	3100	2700	8800	...

between 0.1 and 0.2 dex for most of the abundance ratios determined here.

The effect of random observational errors in the values derived for T_e[N II] and T_e[O III] is estimated to be below ± 400 K for most positions. The exceptions are M20 and M16, objects whose spectra show the lowest signal-to-noise ratio. The most extreme case is M16–2, where an uncertainty of ± 1000 K is estimated. On the other hand, the values of T_e[O III] are likely to be affected by a systematic error due to the blending of [O III] $\lambda 4363$ with [Fe II] $\lambda 4359$ and O II $\lambda 4367$. The contribution of these lines to the total intensity can be $\sim 7\%$ in M42 (Esteban et al. 1998) and $\sim 14\%$ in M8 (Esteban et al. 1999): such contributions imply that the values of T_e[O III] can be 200–300 K lower than those presented here. The effect of this change in T_e[O III] is small for most of the abundance ratios discussed here, and remains below 0.1 dex in any case.

The values found for T_e[O III], T_e[N II] and N_e[Cl III] are presented as a function of N_e[S II] in Fig. 3. No apparent trends can be seen in the relation of N_e[Cl III] with N_e[S II], but both temperatures show loose correlations with the density, which is especially clear for T_e[O III]. These loose correlations are satisfied by areas belonging to different H II regions characterized by various excitation conditions (although sharing similar chemical abundances, as shown below) and could be reflecting a real phenomenon. The temperature in a static nebula is determined by the equilibrium between the heating rate due to ionization and the cooling rate due to recombination processes and the nebular radiation, mainly the collisionally excited line radiation. At a given metallicity, the value of the equilibrium temperature is rather insensitive to the stellar radiation field (Osterbrock 1989), and T_e can be expected to increase with density – as in Fig. 3a and 3b – reflecting the effects of collisional de-excitation on the cooling rate.

All the areas show T_e[O III] $< T_e$[N II]. This result is usually obtained for H II regions and is generally accepted as real, it being considered a consequence of both the hardening of the radiation field in the lower ionization zones where the [N II] lines are emitted and the low concentration in these zones of O^{++}, whose fine-structure transitions cool the gas very efficiently (Stasińska 1980).

6. Ionic abundances

The ionic abundances have been derived with the usual assumption that the line emission originates in a layer characterized by single values for the density (given by N_e[S II]) and the temperature. The values of T_e[N II] have been used to determine the abundances of those ions with low ionization degree: O^+, N^+, S^+, Cl^+ and Ni^{++}. The values of T_e[O III] have been used (when available, T_e[N II] otherwise) to determine the rest of the ionic abundances: O^{++}, S^{++}, Cl^{++}, Ar^{++}, Ar^{3+}, He^+ and C^{++}. The intensity ratios used to determine the ionic abundances relative to H^+ are listed in Table 4.

H I emissivities have been taken from Hummer & Storey (1987), the emissivities for the forbidden lines (excluding [Cl II] $\lambda 8579$ and the Ni lines) have been calculated with the IRAF *nebular* package, with the atomic parameters referenced therein (version of 1997 May).

The atomic data for Cl^+ (not considered in IRAF) have been taken from the compilation by Mendoza (1983).

The lines [Ni II] $\lambda\lambda 7378$, 7412 and [Ni III] $\lambda 7890$ could be measured in some objects, but the determination of the Ni abundance is hampered by several problems. Both [Ni II] lines are severely affected by fluorescence effects (Lucy 1995). On the other hand, there are no calculations in the literature for the collision strengths of Ni^{++}, although Osterbrock et al. (1992) present some estimates based on the collision strengths of Fe^{6+}. Furthermore, the [Ni III] $\lambda 7890$ line is affected by sky emission, and ionization models – needed to estimate the contribution of Ni^{3+} to the total abundance – do not usually consider the Ni ions. Anyway, the abundance ratio Ni^{++}/H^+ has been calculated with the approximations used by Osterbrock et al. (1992),

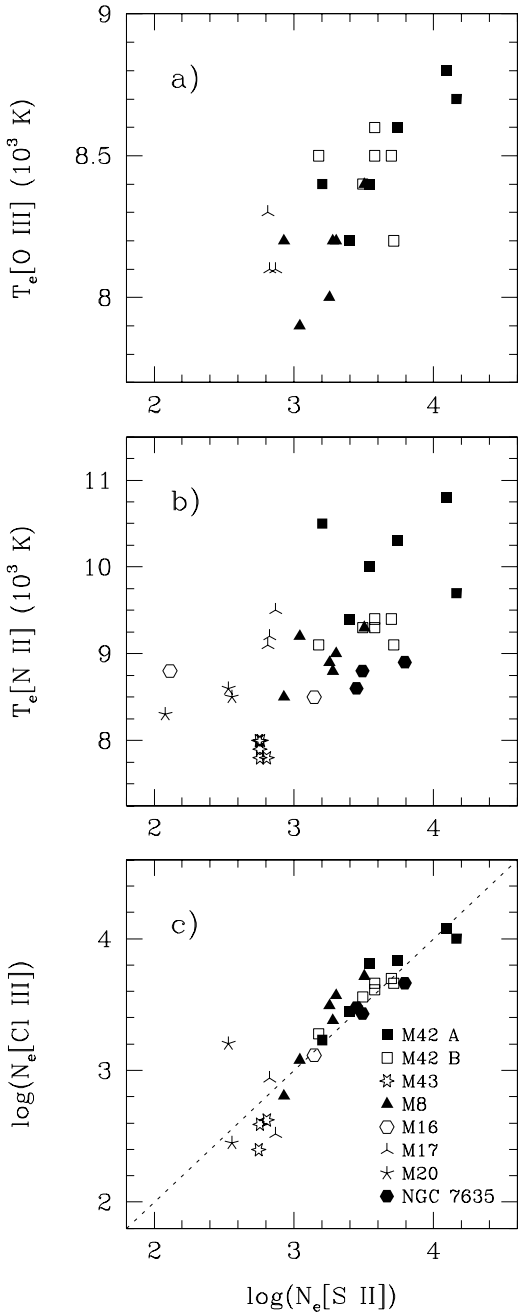

Fig. 3a–c. The values obtained for T_e[O III] **a**, T_e[N II] **b** and N_e[Cl III] **c** as a function of N_e[S II]. The dashed line in **c** represents the equality N_e[Cl III] = N_e[S II]

but these values must be considered with caution and no attempt will be made to determine the total Ni abundance.

The abundance ratio C^{++}/H^+ has been obtained from the intensity of the recombination line C II λ4267, using the relationship derived by Peimbert et al. (1995), which is based on the recombination coefficient calculated by Péquignot et al. (1991):

$$C^{++}/H^+ = 0.0898 \left(\frac{T_e}{10^4}\right)^{0.25} \frac{I(\lambda 4267)}{I(H\beta)}. \quad (1)$$

Table 4. Line ratios used in the abundance determination

Ion	Ratio[a]	T_e[b]
O^+.....	I([O II] $\lambda\lambda$7320 + 7330)/I(Pa12)	T_e[N II]
O^{++}.....	I([O III] $\lambda\lambda$4959 + 5007)/$I(H\beta)$	T_e[O III]
S^+.....	I([S II] $\lambda\lambda$6716 + 6731)/$I(H\alpha)$	T_e[N II]
S^{++}.....	I([S III] λ6312)/$I(H\alpha)$	T_e[O III]
Cl^+.....	I([Cl II] λ8579)/I(Pa12)	T_e[N II]
Cl^{++}.....	I([Cl III] λ5538)/$I(H\beta)$	T_e[O III]
N^+.....	I([N II] $\lambda\lambda$6548 + 6583)/$I(H\alpha)$	T_e[N II]
Ar^{++}.....	I([Ar III] λ7136)/I(Pa12)	T_e[O III]
Ar^{3+}.....	I([Ar IV] λ4740)/$I(H\beta)$	T_e[O III]
Ni^{++}.....	I([Ni III] λ7890)/I(Pa12)	T_e[N II]
C^{++}.....	I(C II λ4267)/$I(H\beta)$	T_e[O III]
He^+.....	I(He I λ4471)/$I(H\beta)$,	
	I(He I λ5876)/$I(H\alpha)$,	
	I(He I λ6678)/$I(H\alpha)$	T_e[O III]

[a] Pa12 is severely affected by atmospheric emission in several positions, where Pa13 is used for normalization purposes. The line [Ar III] λ7136 falls in the red range for M42 and M43; the line ratio used for these objects is I([Ar III] λ7136)/$I(H\alpha)$

[b] T_e[N II] is used to derive all the ionic abundances for M43, M16, M20 and NGC 7635, where T_e[O III] is not available

The He I emissivities have been taken from Smits (1991). [Smits (1996) presents more accurate calculations, but the results are very similar to those of Smits (1991) for the lines and physical conditions considered here.] The values derived for He^+/H^+ must be corrected for the effects of collisional excitation and self-absorption. The collisional corrections have been obtained from the empirical formulas given by Clegg (1987); the correction factors are below 17% for the lines used in the abundance determination (λ4471, λ5876 and λ6678). The effective optical depth for self-absorption processes and the corresponding correction factors have been estimated from the calculations of Almog & Netzer (1989). The optical depth adopted for each area is the mean value of those implied by $I(\lambda 7065)/I(\lambda 4471)$ and $I(\lambda 7065)/I(\lambda 5876)$; the correction factors for self-absorption are $\leq$ 3%.

The values obtained for the ionic abundances are listed in Table 5. Note that the values of the abundance ratio He^+/H^+ are not presented for the regions studied in M43. The spectra of this nebula – the only object in the sample which is excited by a B star (NU Ori) – are greatly affected by dust-scattered stellar light, in such a way that some He I lines, like λ4471, λ4713 or λ4922, are completely swallowed up by the stellar absorption lines. The H I lines (mainly Hγ and Hδ) are also affected, but to a much lower degree. A lower limit to the He^+ abundance in M43 has been obtained from the least affected He I lines, λ5876 and λ6678: $He^+/H^+ > 0.015$. On the other hand, the C II line could not be measured in M43. An upper limit to its intensity implies $C^{++}/H^+ < 2\times10^{-5}$, but this value is too low (even for this low-excitation object) and C II λ4267 is probably affected

Table 5. Ionic abundances (X^{i+}/H^+)[a]

Object	O^+	O^{++}	S^+	S^{++}	Cl^+	Cl^{++}	N^+	Ar^{++}	Ar^{3+}	C^{++}	He^+	Ni^{++}
M42 A–1	1.2−4	1.6−4	7.1−7	8.1−6	2.1−8	1.2−7	1.6−5	1.7−6	1.6−8	1.6−4	0.0750	5.0−8
M42 A–2	8.7−5	1.4−4	5.5−7	8.6−6	2.2−8	1.0−7	1.5−5	1.7−6	1.1−8	1.5−4	0.0795	3.9−8
M42 A–3	4.8−5	2.4−4	1.8−7	7.1−6	7.3−9	1.0−7	5.6−6	2.0−6	2.5−8	1.9−4	0.0802	4.0−8
M42 A–4	7.7−5	1.7−4	3.5−7	7.6−6	1.5−8	9.9−8	1.1−5	1.8−6	1.8−8	1.8−4	0.0789	5.8−8
M42 A–5	8.1−5	2.0−4	3.7−7	8.8−6	1.2−8	1.0−7	9.9−6	1.9−6	1.0−8	2.0−4	0.0826	9.0−8
M42 A–6	3.4−5	1.7−4	3.2−7	6.9−6	8.6−9	8.6−8	6.6−6	1.6−6	6.9−9	2.1−4	0.0844	6.6−8
M42 B–1	1.7−4	1.2−4	8.4−7	9.5−6	2.4−8	1.1−7	2.1−5	2.0−6	...	1.8−4	0.0768	4.9−8
M42 B–2	1.5−4	1.3−4	5.1−7	9.0−6	1.4−8	1.1−7	1.7−5	2.1−6	...	1.8−4	0.0817	5.9−8
M42 B–3	1.7−4	1.3−4	6.3−7	9.1−6	1.9−8	1.1−7	1.9−5	2.0−6	...	2.0−4	0.0768	5.6−8
M42 B–4	2.2−4	8.3−5	1.0−6	9.2−6	3.0−8	1.1−7	2.8−5	1.6−6	...	1.4−4	0.0674	6.5−8
M42 B–5	1.5−4	9.5−5	7.2−7	6.5−6	2.4−8	8.5−8	2.0−5	1.4−6	...	1.9−4	0.0686	5.6−8
M42 B–6	2.0−4	1.3−4	1.0−6	1.1−5	2.7−8	1.3−7	2.5−5	2.0−6	...	1.7−4	0.0715	4.8−8
M43–1[b]	2.5−4	7.4−6	2.2−6	4.2−6	7.1−8	5.7−8	4.2−5	1.0−7	...	...	...	3.2−7
M43–2	2.7−4	1.0−5	3.3−6	4.0−6	9.5−8	5.0−8	4.3−5	1.1−7	...	...	...	4.8−7
M43–3	3.8−4	3.0−5	3.5−6	2.8−6	1.0−7	4.5−8	4.4−5	3.1−7	...	...	...	1.0−6
M43–4	2.7−4	7.9−6	2.4−6	4.3−6	6.9−8	6.1−8	4.5−5	1.1−7	...	...	...	...
M43–5	2.8−4	9.6−6	2.0−6	5.7−6	6.0−8	7.1−8	4.3−5	4.8−7	...	...	...	...
M8–1	1.7−4	6.0−5	4.9−7	8.7−6	1.8−8	1.1−7	1.7−5	1.9−6	...	1.6−4	0.0773	4.9−8
M8–2	2.3−4	8.2−5	6.7−7	1.1−5	2.3−8	1.1−7	2.4−5	2.1−6	...	2.3−4	0.0708	4.3−8
M8–3	1.7−4	6.9−5	5.5−7	8.1−6	1.9−8	1.1−7	1.9−5	1.9−6	...	1.7−4	0.0775	4.7−8
M8–4	1.7−4	8.3−5	5.0−7	8.3−6	1.5−8	1.0−7	1.7−5	1.9−6	...	2.1−4	0.0801	4.4−8
M8–5	1.6−4	1.0−4	3.8−7	8.6−6	...	8.8−8	1.2−5	1.8−6	...	2.1−4	0.0850	...
M8–6	1.1−4	1.1−4	5.1−7	9.0−6	1.7−8	1.1−7	1.5−5	1.9−6	...	2.0−4	0.0800	5.2−8
M16–1	1.8−4	5.6−5	2.0−6	4.3−6	3.9−8	7.4−8	4.3−5	1.2−6	...	1.7−4	0.0758	...
M16–2	7.2−5	7.7−5	3.4−7	3.0−6	...	6.0−8	9.5−6	1.1−6	...	2.3−4	0.0910	...
M17–1	5.5−5	2.4−4	2.1−7	5.9−6	3.8−9	8.3−8	4.4−6	1.7−6	2.9−8	5.4−4	0.0906	...
M17–2	4.7−5	3.0−4	1.9−7	8.0−6	...	1.1−7	4.1−6	2.1−6	4.1−8	3.3−4	0.0933	...
M17–3	5.2−5	2.9−4	1.6−7	7.6−6	3.9−9	1.1−7	3.4−6	2.0−6	3.3−8	3.9−4	0.0926	...
M20–1	1.3−4	3.9−5	1.3−6	3.9−6	3.0−8	7.4−8	2.3−5	1.1−6	...	9.4−5	0.0723	...
M20–2	1.5−4	5.9−5	1.0−6	5.2−6	3.4−8	7.2−8	2.1−5	1.3−6	...	2.4−4	0.0816	...
M20–3	1.4−4	1.9−5	2.1−6	4.1−6	5.6−8	5.7−8	3.6−5	6.8−7	...	8.5−5	0.0541	...
NGC 7635–1	2.4−4	2.0−5	2.1−6	6.1−6	6.3−8	9.2−8	3.3−5	8.2−7	...	...	0.0572	...
NGC 7635–2	2.3−4	4.2−5	1.6−6	6.6−6	4.5−8	9.3−8	2.7−5	1.0−6	...	1.7−4	0.0657	...
NGC 7635–3	1.9−4	3.8−5	1.6−6	6.8−6	3.9−8	9.9−8	2.7−5	8.8−7	...	1.3−4	0.0578	...

[a] Expressions like 1.2−4 stand for 1.2×10^{-4}
[b] $He^+/H^+ > 0.015$ and $C^{++}/H^+ < 2 \times 10^{-5}$ in M43 (see text)

by the corresponding absorption feature in the dust-scattered stellar spectrum.

7. Ionization models

In principle, O is the only element for which we can observe in the optical range all the ionization states expected to be present inside H II regions: O^+ and O^{++}. These nebulae are not expected to contain a significant number of photons with enough energy to ionize O^{++}, a fact confirmed by the absence from their spectra of He II lines (like He II λ4686), since He^{++} and O^{3+} require similar energies to be produced (54.4 and 54.9 eV, respectively).

To derive the total abundances for the other elements, it is necessary to estimate the contribution of the unobserved ions. These estimates can be made using ionization models, but the results of these models depend on poorly known parameters like the characteristics of the ionizing radiation field and the nebular structure. This dependence can be minimized by using model grids (where each model is characterized by the number of ionizing stars, the stellar effective temperatures, $T_{\rm eff}$, and the density and metallicity of the gas) to study the relative variations of the ionization fractions of the element of interest and a reference element with two observed ions whose ionization potentials are similar to those of the first element. This can be a good approximation, but it must be taken into account that the ionization equilibrium for the different ions is affected by factors which are not always well known, like the detailed dependence on energy of the ionization and recombination coefficients and the effects of charge-exchange reactions.

Three series of ionization models have been considered: those from Rubin (1985), Stasińska (1990) and Gruenwald &

Viegas (1992). None of these authors considers the effects of dust on his calculations, but dust absorption cross-sections are expected to behave in a hydrogenic fashion in such a way that dust will not significantly alter the ionization balance between the different ions (Mathis 1986). The ionization models of the different authors can differ in the model atmospheres used, the values adopted for the atomic data, the kind of atomic processes considered, etc. Therefore, when the results of these models differ from each other or from the observational data, it is difficult to infer the reasons and no attempt will be made to do so in this paper. However, there is one characteristic of the work of Gruenwald & Viegas (1992) that can be significant: their results are presented for several lines of sight across each model, a better approach to resolved sources than the models just giving the volume-averaged ionic fractions.

The models selected from Gruenwald & Viegas (1992) are those with solar metallicities $Z_\odot$ or $Z_\odot/3$; these models are ionized by a single star with $T_{\rm eff} = 30\,900$ or $50\,000$ K and have densities $N_{\rm e} = 10$, 100, or 1000 cm^{-3}. The models selected from Stasińska (1990) have metallicities $Z_\odot$ or $Z_\odot/2$, are ionized by 1, 10^2 or 10^4 stars with $T_{\rm eff} = 32\,500$–$55\,000$ K and have densities $N_{\rm e} = 10$ or 1000 cm^{-3}. Two series of models have been selected from Rubin (1985), both with 10^{49} Lyman-continuum photons per second. The first series is characterized by solar abundances, $T_{\rm eff} = 31\,000$–$40\,000$ K and $N_{\rm e} = 100$, 1000, or $10\,000$ cm^{-3}. The second series is characterized by 'nebular' abundances, $T_{\rm eff} = 33\,000$ or $40\,000$ K and mean densities $N_{\rm e} = 100$, 1000, or $10\,000$ cm^{-3}, but including clumps denser by a factor of 10.

8. Reference abundances

The total abundances implied by the data will be compared to the Solar System abundances, since these are those known with the highest precision and for the greatest number of elements. Both the solar and meteoritic values have been taken from the compilation of Grevesse et al. (1996).

On the other hand, several recent results on the abundances of elements like O, C, N and Kr relative to H in the interstellar medium and in B stars of the solar neighbourhood, are being interpreted as evidence that these abundance ratios are only about $2/3$ of the solar values (Snow & Witt 1996; Cardelli & Meyer 1997; Sofia et al. 1997 and references therein). Therefore, the resulting abundances will be also compared with those characteristic of B stars. The values used here have been taken from Snow & Witt (1996) and represent the mean value of the abundances derived by several authors for stars in the solar neighbourhood, mainly B-type stars.

The elements C and O – the most abundant after H and He – may preferentially condense into dust grains; but still most of their atoms remain in the gaseous phase. Their abundances have been measured towards several lines of sight in the solar neighbourhood, and show similar values, implying that their degree of incorporation into dust grains is quite constant, at least outside the densest molecular clouds (Cardelli et al. 1996 and references therein). These interstellar values will be compared to the nebular abundances.

In general, the resulting nebular abundances will not be compared with the results obtained by other authors for the H II regions studied here, since the different determinations of the ionic abundances lead to similar results (at least for nebular areas characterized by similar ionization conditions), whereas the values of the total abundances depend on the ionization-correction factors assumed in each case.

9. Discussion

9.1. *The abundances of* O, S *and* Cl

The values of $\mathrm{O/H} = \mathrm{O^+/H^+ + O^{++}/H^+}$ are shown in Fig. 4. The main source of errors in this determination of the O abundance – excluding those inherent in the method – is introduced by the lines used to derive $\mathrm{O^+/H^+}$ ([O II] λ7320+30) since they are very sensitive to errors in the temperature and are severely affected by sky subtraction in several positions, namely M16–2 and M20–1, 2 and 3. These positions are precisely those where the signal-to-noise ratio is rather low for many lines, and their calculated ionic abundances have the greatest uncertainties. Taking into account these considerations, which reduce the reliability of the values found for O/H in M16–2 and M20, the results are compatible with a total abundance $\log(\mathrm{O/H}) \sim -3.55 \pm 0.1$ for all the objects in the sample, although the uncertainty of this value is difficult to estimate. This abundance ratio is the most sensitive of those presented here to errors in the temperature: a change of ± 500 K in $T_{\rm e}$ would lead to changes in O/H of ± 0.1 dex and ± 0.2 dex for the positions with higher and lower ionization degree respectively. Anyway, the conclusion of a constant O abundance to within the observational errors seems solid enough and suggests that the other abundance ratios must also be similar in all the objects. This will be used as a working assumption hereafter.

The values obtained for $\log(\mathrm{S^+/H^+ + S^{++}/H^+})$ and $\log(\mathrm{Cl^+/H^+ + Cl^{++}/H^+})$ are presented as a function of $\log(\mathrm{O^+/O^{++}})$ in Fig. 5, where $\mathrm{S^+/S^{++}} = 0.02$–$1.25$ and $\mathrm{Cl^+/Cl^{++}} = 0.04$–$2.22$. The small symbols in Fig. 5 show the predictions of the ionization models listed in Sect. 7 after scaling them to reach the best agreement between observations and models: $\log(\mathrm{S/H}) = -5.00$ and $\log(\mathrm{Cl/H}) = -6.85$.

The observational results and the models are compatible with the presence of small quantities of $\mathrm{S^{3+}}$ (produced at 34.8 eV) and $\mathrm{Cl^{3+}}$ (produced at 39.6 eV) in the areas with high ionization degree. The line [S IV] 10.51 μm has been measured by Simpson et al. (1998) in spectra of M42 that sample almost all the ionized nebula. They determine $\mathrm{S^{3+}/H^+} = 6.3 \times 10^{-7}$ (and $\mathrm{S^{++}/H^+} = 7.5 \times 10^{-6}$ from [S III] 18.71 μm). This small contribution of $\mathrm{S^{3+}}$ to the total abundance can account for the observed decrease in $(\mathrm{S^+/H^+ + S^{++}/H^+})$ in some areas of M42 A and in M17 and therefore agrees with the observations and the ionization models. On the other hand, there is a weak feature in the spectra of M42 A that could be [Cl IV] λ8046. The intensity of this feature implies $\mathrm{Cl^{3+}/(Cl^+ + Cl^{++})} \sim 0.02$, suggesting that the contribution of $\mathrm{Cl^{3+}}$ to the total abundance

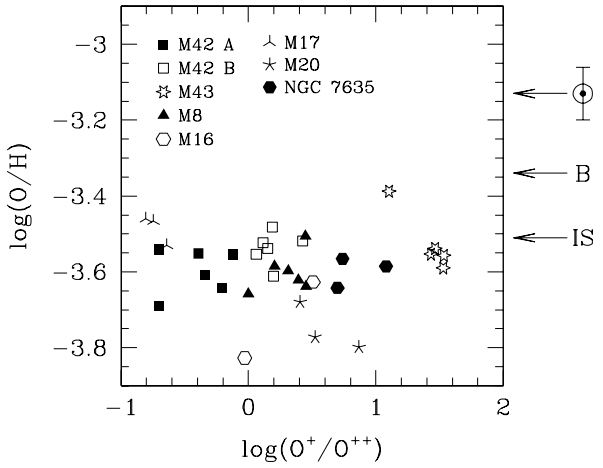

Fig. 4. The abundance ratio $\mathrm{O/H} = \mathrm{O^+/H^+ + O^{++}/H^+}$ as a function of the ionization degree. The symbols to the right of the diagram represent the solar value ($\odot$), a value representative of stars in the solar neighbourhood (B) and the mean interstellar value (IS) along several lines of sight (references in the text). [Note that we can obtain an upper limit to the fraction of O atoms depleted in dust by considering the limitations imposed by the abundances of those elements like Fe, Si and Mg, which react with O to form compounds that can survive in the diffuse interstellar medium (different kinds of oxides and silicates). Cardelli et al. (1996) determine that a maximum of $\mathrm{O/H} \simeq 1.8\times10^{-4}$ can be in dust. Since the interstellar abundance is $\mathrm{O/H} \simeq 3.1\times10^{-4}$, the total (gas and dust) abundance must be $\mathrm{O/H} \simeq 4.9\times10^{-4}$, a value consistent with the abundances measured in B stars.]

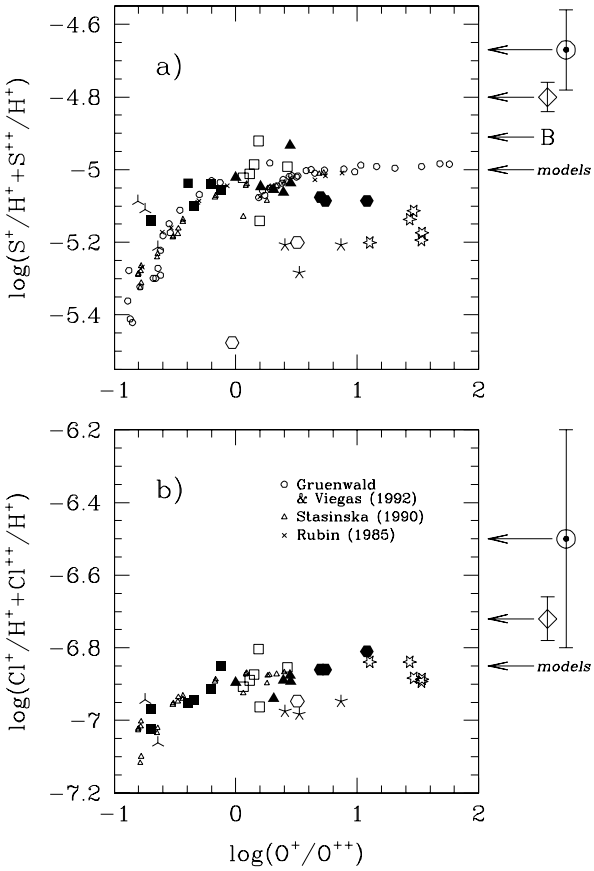

Fig. 5a and b. The abundance ratios $\log(\mathrm{S^+/H^+ + S^{++}/H^+})$ **a** and $\log(\mathrm{Cl^+/H^+ + Cl^{++}/H^+})$ **b** as a function of $\log(\mathrm{O^+/O^{++}})$. The large symbols representing the different H II regions are identified in Fig. 4. The small symbols show the predictions of several ionization models (identified in the lower panel) for the variations of $\log(x(\mathrm{S^+}) + x(\mathrm{S^{++}}))$ and $\log(x(\mathrm{Cl^+}) + x(\mathrm{Cl^{++}}))$ as a function of $\log(x(\mathrm{O^+})/x(\mathrm{O^{++}}))$, where $x(\mathrm{ion})$ is the ionization fraction of the corresponding ion. The models have been scaled to the indicated abundance values. The diamonds at the right of the diagrams represent the meteoritic abundances, the other symbols are identified in Fig. 4

is negligible for all the regions studied and cannot explain the slight but noticeable decrease of $(\mathrm{Cl^+/H^+ + Cl^{++}/H^+})$ with the ionization degree. Noting that the collision strengths for $\mathrm{Cl^+}$ (Krueger & Czyzak 1970) are considered to have high uncertainties ($\sim$ 40% according to Mendoza 1983), a possible explanation would be an error in the ratio $\mathrm{Cl^+/H^+}$. If the real values of $\mathrm{Cl^+/H^+}$ were 40% lower than those calculated, all the regions would show a total abundance $\log(\mathrm{Cl/H}) \simeq -6.95$. Furthermore, note that in such case, the ionization fractions of $\mathrm{Cl^+}$ and $\mathrm{S^+}$ would be similar, as can be expected from the values of their ionization potentials (23.8 and 23.2 eV, respectively).

As for the low excitation objects, the positions in NGC 7635 and M43 show unexpected underabundances in the S ratio. The line used to derive the $\mathrm{S^{++}}$ abundance ([S III] λ6312) is, excluding [O II] $\lambda7320+30$, the feature most sensitive to errors in the temperature: a change of ±500 K in T_e would lead to changes in $(\mathrm{S^+/H^+ + S^{++}/H^+})$ of up to ±0.13 dex. [The effect of this change in T_e would be $\leq \pm0.1$ dex for $(\mathrm{Cl^+/H^+ + Cl^{++}/H^+})$ and the rest of the ratios discussed hereafter.] Therefore, the decrease of the S ratio for the lower-ionization areas could be due to a systematic error in the temperature mainly affecting the S results. Note that only T_e[N II] is available for deriving ionic abundances in NGC 7635 and M43, and that $\mathrm{S^+}$ and $\mathrm{S^{++}}$ have comparable contributions to the S abundance in these objects. The $\mathrm{S^{++}}$ emitting region can be characterized by temperatures below those found with the [N II] lines, which would increase the derived $\mathrm{S^{++}/H^+}$ ratio. The effect could also be due to a failure in the simple assumption of a two-layer emitting region.

Anyway, models and observations agree on $\mathrm{S/H} = (\mathrm{S^+/H^+ + S^{++}/H^+})$ and $\mathrm{Cl/H} = (\mathrm{Cl^+/H^+ + Cl^{++}/H^+})$ when $\mathrm{O^+/O^{++}} > 1$, so that we can compare the total abundances of O/H, S/H and Cl/H for the regions of lower excitation. The behaviour of the three abundance ratios for $\mathrm{O^+/O^{++}} > 1$ – showing greater spread when the sensitivity to the temperature is higher – agrees with the previous assumption that the values of O/H, S/H and Cl/H are very similar for all the H II regions considered.

9.2. The abundances of N *and* Ar

The variations of $\mathrm{N^+/H^+}$ and $\mathrm{Ar^{++}/H^+}$ as a function of $\mathrm{O^+/O^{++}}$ are shown in Fig. 6, along with the predictions of the ionization models scaled to $\log(\mathrm{N/H}) = -4.4$ and

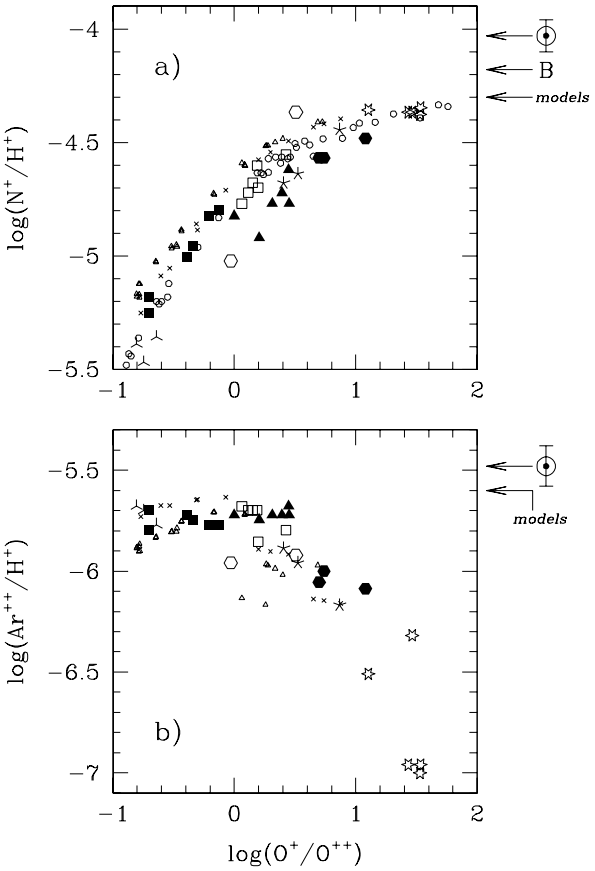

Fig. 6a and b. The ratios $\log(N^+/H^+)$ **a** and $\log(Ar^{++}/H^+)$ **b** as a function of $\log(O^+/O^{++})$. The large symbols represent the different H II regions and are identified in Fig. 4. The small symbols show the predictions of the ionization models identified in Fig. 5b for the variations of $\log(x(N^+))$ and $\log(x(Ar^{++}))$ as a function of $\log(x(O^+)/x(O^{++}))$. The models have been scaled to $\log(N/H) = -4.3$ and $\log(Ar/H) = -5.6$. The symbols at the right of the diagrams are identified in Fig. 4

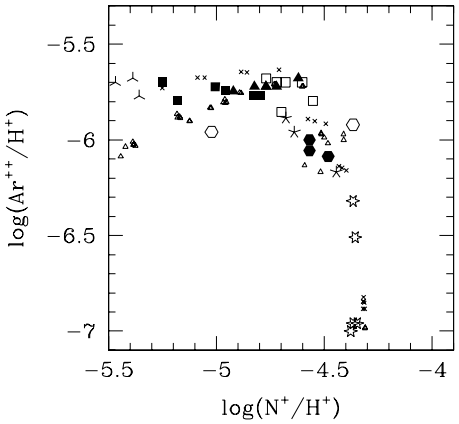

Fig. 7. The abundance ratio $\log(N^+/H^+)$ as a function of $\log(Ar^{++}/H^+)$. The symbols are identified in Figs. 4 and 5b. The models have been scaled to $\log(N/H) = -4.3$ and $\log(Ar/H) = -5.6$

$\log(Ar/H) = -5.6$. The contribution of Ar^{3+} (produced at 40.7 eV) to the Ar abundance can be neglected, since the ratio Ar^{3+}/H^+ could be calculated in the positions with high ionization degree (M42 A and M17), and implies $Ar^{3+}/Ar^{++} \sim 0.01$ (see Table 5). The models fit reasonably well the variation of N^+/H^+ with O^+/O^{++}, suggesting that the value of N/H is similar for all the objects. However, models and observations disagree in the relation of Ar^{++} with O^+/O^{++}. The ionization models predict that the contribution of Ar^{3+} to the total abundance should be greater than that measured; the models of Stasińska (1990) predict a value as high as $Ar^{3+}/Ar \sim 0.2$ for the positions with high ionization degree. For those regions where $O^+/O^{++} > 1$, the disagreement is greater and arises from the predicted contribution of Ar^+ to the total abundance. This disagreement could be due to the fact that the ions O^+/O^{++} and Ar^+/Ar^{++} form at different conditions: the ratio O^+/O^{++} is inversely proportional to the number of photons with energies above 35.1 eV, whereas the ionization potential of Ar^+ is 27.6 eV (the ionization potential of N^+, showing better agreement with the ionization models in Fig. 6, is 29.6 eV). The ionization conditions giving rise to N^+/N^{++} and Ar^+/Ar^{++} are truly similar, and the models fit much better the behaviour of Ar^{++}/H^+ with respect to N^+/H^+, as shown in Fig. 7.

On the other hand, the ratio Ar^+/H^+ has been calculated by Simpson et al. (1998) in M42 using [Ar II] 6.99 μm: they find $Ar^+/H^+ = 4.6 \times 10^{-7}$ (and $Ar^{++}/H^+ = 2.04 \times 10^{-6}$ from [Ar III] 8.99 μm, a value similar to those measured here for M42). Taking this into account, the results found here for N and Ar imply that $\log(N/H) = -4.3$ and $\log(Ar/H) = -5.6$ in all the objects studied.

9.3. The abundances of C *and* He

If we continue using the ratio O^+/O^{++} as a reference for the variation of the ionization degree, the disagreement between observations and models increases for C^{++} (produced at 24.4 eV) and He^+ (produced at 24.6 eV), as can be seen in Fig. 8. [The predictions of ionization models have been set arbitrarily to the solar abundances in this figure.] The ratio Cl^+/Cl^{++}, whose variation reflects mainly the contribution of Cl^+ (with ionization potential of 23.8 eV), might be more adequate. In fact, the results for C^{++}/H^+ and He^+/H^+ are clearly related to those for Cl^+/Cl^{++}, as shown in Fig. 9, but the only models that consider Cl (Stasińska 1990), do not reproduce these relations. Note that the results of ionization models can be expected to be more uncertain for those ions whose ionization potentials are relatively high or low, making their ionization fractions more sensitive to the assumed shape of the radiation field and the density structure of the nebula.

The tight relation between He^+/H^+ and Cl^+/Cl^{++} implies that the He abundance must be the same in all the H II regions studied. However, the disagreement of the ionization models with the observations prevents us from obtaining the real abundance, and only a lower limit can be deduced from the observational results: $He/H \geq 0.093$. The case of C^{++} is somewhat more complicated, since the relation between

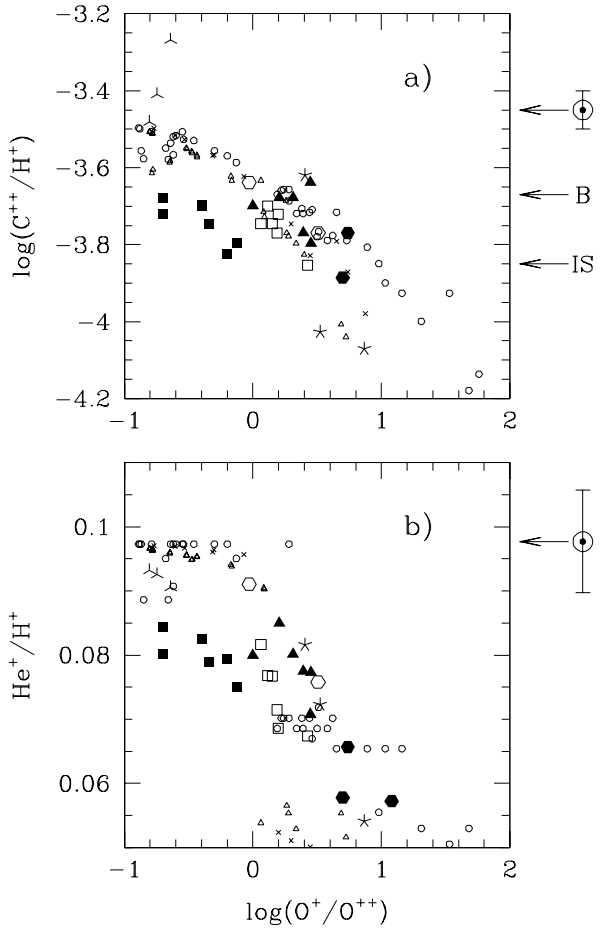

Fig. 8a and b. The abundance ratios $\log(C^{++}/H^{+})$ **a** and He^{+}/H^{+} **b** as a function of $\log(O^{+}/O^{++})$. The large symbols represent the different H II regions and are identified in Fig. 4. The small symbols are identified in Fig. 5b and show the predictions of several ionization models. The models have been scaled to the solar abundances: $\log(C/H) = -3.45$ and $He/H = 0.0977$. The symbols at the right of the diagrams are identified in Fig. 4

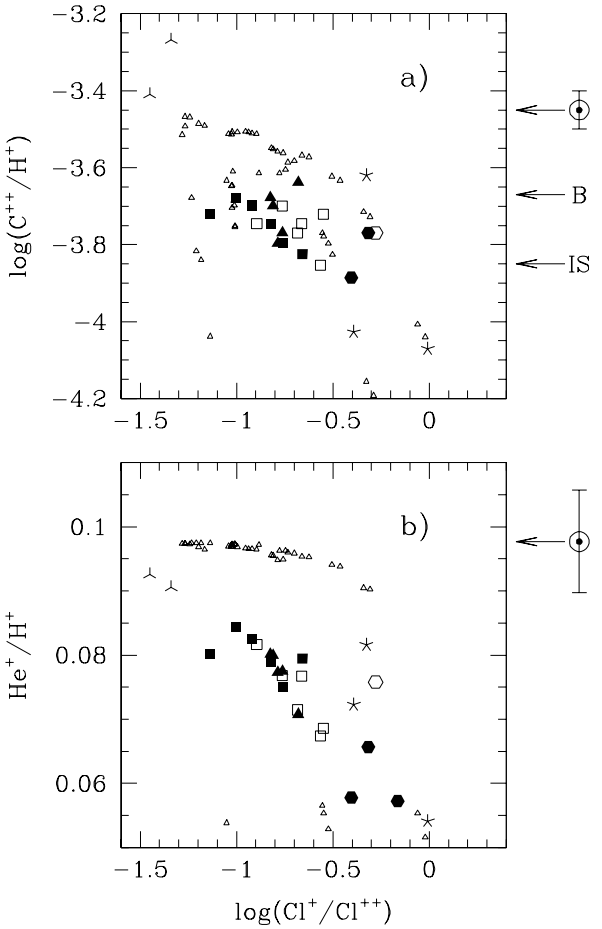

Fig. 9a and b. The ratios $\log(C^{++}/H^{+})$ **a** and He^{+}/H^{+} **b** as a function of $\log(Cl^{+}/Cl^{++})$. The models have been scaled to the solar abundances. The symbols are identified in Figs. 4 and 5b

$\log(C^{++}/H^{+})$ and $\log(Cl^{+}/Cl^{++})$ is not as clear as for He^{+}. Taking into account the constant abundances deduced for He and the other elements, we could conclude that the results presented in Fig. 9a imply $\log(C/H) \simeq -3.3$ in all the objects studied, but the possibility suggested by the models cannot be excluded: $\log(C/H) = -3.6$ in general, and an overabundance in M17.

The ratio C^{++}/H^{+} is the only one of those derived here implying abundances above solar (at least for M17). This could be due to the fact that a recombination line is being used to derive this ratio. Several studies show that the abundances derived for ions like O^{++} and C^{++} using recombination lines are higher than those obtained from forbidden transitions (e.g. Peimbert et al. 1993; Esteban et al. 1998, 1999). The C abundance has been derived in M42 and M8 using the collisionally excited lines C II] λ2326 and C III] λ1908. The resulting abundances, $\log(C^{+}/H^{+} + C^{++}/H^{+}) \simeq -4.0$ in M42 (Walter et al. 1992) and $\log(C^{+}/H^{+} + C^{++}/H^{+}) \simeq -3.8$ in M8 (Peimbert et al. 1993), are clearly below the value of C^{++}/H^{+} obtained from C II λ4267, with a factor of 2–3 difference in the C^{++} abundance implied by recombination and collisionally excited lines. These discrepancies are usually attributed to small-scale spatial temperature variations, that would critically affect the abundances derived from the intensity ratio of a line excited collisionally and a recombination line. The effect of considering these temperature variations would be an increase of ~ 0.2 dex in those abundances relative to H derived here from forbidden lines. On the other hand, several objections have been raised to the existence of strong temperature fluctuations in nebulae, such as (i) the similarity in the abundance ratios derived from optical forbidden lines and temperature-insensitive infrared forbidden lines and (ii) the extreme differences (up to a factor of 15) found between the C^{++}/H^{+} abundance ratio as derived from recombination and collisionally excited lines in some planetary nebulae (see, for example, Liu 1998). Taken at face value, these objections suggest that the abundances derived from recombination lines may not be reliable. Note that if the values derived here for C^{++}/H^{+} were scaled down (by factors of 2–3) to the values implied by the collisionally excited ultraviolet lines, the results would imply values for the C abundance close to the

interstellar value, in accord with the evidence of the presence of dust grains inside H II regions mixed with the ionized gas (Münch & Persson 1971; Osterbrock 1989; Rodríguez 1996, 1999 in preparation).

10. Conclusions

The spectra of several positions inside seven Galactic H II regions have been used to obtain an homogeneous set of data comprising temperatures (T_e[O III] and T_e[N II]) densities (N_e[Cl III] and N_e[S II]) and the abundances of O^+, O^{++}, S^+, S^{++}, Cl^+, Cl^{++}, N^+, Ar^{++}, C^{++} and He^+. These data have been used to study the trends followed by temperatures, densities and the ionization fractions of different elements. The relative behaviour of the calculated ionic abundances by itself, without any assumptions concerning the ionization correction factors, implies that the chemical abundances are similar in all the H II regions studied. The preferred values for the abundances, within ± 0.1 dex, are: $\log(O/H) = -3.55$, $\log(S/H) = -5.0$, $\log(Cl/H) = -6.85$, $\log(N/H) = -4.3$ and $\log(Ar/H) = -5.6$, whereas $He/H \geq 0.093$. All these abundance ratios are below the solar values, but are similar to the abundances derived in B stars and the interstellar medium.

The main result of this work is that – regardless of the real values of the abundances, which can be affected by errors in the temperatures, the atomic data or the method used – all the H II regions studied are characterized by similar abundances. Whenever there are discrepancies, these can be attributed to uncertainties related to the temperature or to a low signal-to-noise in the corresponding spectrum. Taking into account that all the objects considered have galactocentric distances in the range 6–10 kpc, this result does not preclude the existence of a Galactic abundance gradient: it has even been suggested (Simpson et al. 1995) that the galactocentric variations of N/O, N/H and S/H in H II regions with galactocentric distances below 10 kpc can be better explained by a step fit with two levels (such that $\log(N/H) = -4.22$ and $\log(S/H) = -5.12$ from 6 to 10 kpc) than with the usual fit to a linear gradient. The presence of a flat gradient over this range of galactocentric distances is also suggested by several studies on the abundances of O in B-type stars (e.g. Smartt & Rolleston 1997), although its reality is still a matter of debate (e.g. Gummersbach et al. 1998). The results presented here are consistent with the flattening or mild variation of the Galactic abundance gradient in the range 6–10 kpc for all the elements whose total abundances have been estimated or constrained: He, O, S, Cl, N and Ar.

Acknowledgements. I thank Guido Münch and Antonio Mampaso for their advice during the development of this project and their very helpful comments and suggestions, which have improved this manuscript. I also thank Terry Mahoney for revising the English text.

References

Almog Y., Netzer H., 1989, MNRAS 238, 57
Baluja K.L., Burke P.G., Kingston A.E., 1980, J. Phys. B 13, 829
Baluja K.L., Burke P.G., Kingston A.E., 1981, J. Phys. B 14, 119
Cardelli J.A., Meyer D.M., 1997, ApJ 477, L57
Cardelli J.A., Clayton G.C., Mathis J.S., 1989, ApJ 345, 245
Cardelli J.A., Meyer D.M., Jura M., Savage B.D., 1996, ApJ 467, 334
Clegg R.E.S., 1987, MNRAS 229, 31P
Esteban C., Peimbert M., Torres-Peimbert S., Escalante V., 1998, MNRAS 295, 401
Esteban C., Peimbert M., Torres-Peimbert S., García-Rojas J., Rodríguez M., 1999, ApJS 120, 113
Grevesse N., Noels A., Sauval A.J., 1996, In: Holt S.S., Sonneborn G. (eds.) Cosmic Abundances. ASP Conf. Ser. Vol. 99, ASP, San Francisco, p. 117
Gruenwald R.B., Viegas S.M., 1992, ApJS 78, 153
Gummersbach C.A., Kaufer A., Schäfer D.R., Szeifert T., Wolf B., 1998, A&A 338, 881
Hummer D.G., Storey P.J., 1987, MNRAS 224, 801
Krueger T.K., Czyzak S.J., 1970, Proc. R. Soc. London A, 318, 531
Lennon D.J., Burke V.M., 1994, A&AS 103, 273
Liu X.-W., 1998, MNRAS 295, 699
Lucy L.B., 1995, A&A 294, 555
Mathis J.S., 1986, PASP 98, 995
Mendoza C., 1983, In: Flower D.R. (ed.) IAU Symp. 103, Planetary Nebulae. Kluwer, Dordrecht, p. 143
Münch G., Persson S.E., 1971, ApJ 165, 241
Münch G., Wilson O.C., 1962, Zeitschr. Astrophys. 56, 127
Osterbrock D.E., 1989, Astrophysics of Gaseous Nebulae and Active Galactic Nuclei. Univ. Science Books, Mill Valley
Osterbrock D.E., Tran H.D., Veilleux S., 1992, ApJ 389, 305
Peimbert M., Torres-Peimbert S., Dufour R.J., 1993, ApJ 418, 760
Peimbert M., Torres-Peimbert S., Luridiana V., 1995, Rev. Mex. Astron. Astrofís. 31, 131
Péquignot D., Petitjean P., Boisson C., 1991, A&A 251, 680
Pradhan A.K., Gallagher J., 1992, At. Data Nucl. Data Tables 52, 227
Rodríguez M., 1996, A&A 313, L5
Rodríguez M., 1999, A&A 348, 222
Rubin R.H., 1985, ApJS 57, 349
Seaton M.J., 1975 MNRAS 170, 475
Simpson J.P., Colgan S.W.J., Rubin R.H., Erickson E.F., Haas M.R., 1995, ApJ 444, 721
Simpson J.P., Witteborn F.C., Price S.D., Cohen M., 1998, ApJ 508, 268
Smartt S. J., Rolleston W.R.J., 1997, ApJ 481, L47
Smits D.P., 1991, MNRAS 248, 193
Smits D.P., 1996, MNRAS 278, 683
Snow T.P., Witt A.N., 1996, ApJ 468, L65
Sofia U.J., Cardelli J.A., Guerin K.P., Meyer D.M., 1997, ApJ 482, L105
Stafford R.P., Bell K.L., Hibbert A., Wijesundera W.P., 1994, MNRAS 268, 816
Stasińska G., 1980, A&A 85, 359
Stasińska G., 1990, A&AS 83, 501
Walter D.K., Dufour R.J., Hester J.J., 1992, ApJ 397, 196